Swelling, Compression and Tribological Behaviors of Bentonite-Modified Polyacrylate-Type Hydrogels

S. Korres,[1,2] L. Sorochynska,[3] S. Grishchuk,[3] J. Karger-Kocsis[4,5]

[1]*Karlsruhe Institute of Technology, IZBS-Institut für Zuverlässigkeit von Bauteilen und Systemen, Karlsruhe D-76131, Germany*
[2]*Fraunhofer-Institute for Mechanics of Materials (IWM), Freiburg D-79108, Germany*
[3]*Institut für Verbundwerkstoffe GmbH (Institute for Composite Materials), Kaiserslautern University of Technology, Kaiserslautern D-67663, Germany*
[4]*Polymer Technology, Faculty of Engineering and the Built Environment, Tshwane University of Technology, Pretoria 0001, Republic of South Africa*
[5]*Polymer Engineering, Faculty of Mechanical Engineering, Budapest University of Technology and Economics, Budapest H-1111, Hungary*

Received 25 January 2010; accepted 26 April 2010
DOI 10.1002/app.32706
Published online 30 July 2010 in Wiley Online Library (wileyonlinelibrary.com).

ABSTRACT: Hydrogel was synthesized from acrylamide and 2-acryloylamido-2-methylpropanesulfonic acid monomers (ratio: 50/50 wt %) and crosslinked with 0.25 wt % of methylene-bisacrylamide. This hydrogel was also modified by adding 4 wt % of sodium bentonite (NB). Selected properties of the hydrogels with and without NB were investigated and compared. Their water uptake was measured gravimetrically; the compression and compression creep were assessed by dynamic-mechanical and thermomechanical analysis (DMA and TMA, respectively) techniques. The friction and wear of the hydrogels were determined in a shaft(metal)-on-plate(hydrogel) type testing configuration under water lubrication. The hydrogel was transparent and exhibited very high equilibrium water content (>99 wt %). The latter was less affected; however, the hydrogel became slightly more hazy after NB incorporation. The crosslink density of the hydrogels was deduced from swelling and compression tests and compared with the theoretical values. Modification by NB enhanced the ultimate compression strength and reduced the related compression strain. The compression creep response under both loading and deloading strongly depended on the level of the initial load. A very low friction coefficient ($\sim$ 0.003) and a relatively high specific wear rate ($\sim$ 0.05 $mm^3/N\ m$) were registered under water lubricated sliding wear using a metallic counterpart with high surface roughness. Scanning electron microscopy combined with energy dispersive spectroscopy delivered additional information on the NB dispersion and surface structure of the hydrogels. © 2010 Wiley Periodicals, Inc. J Appl Polym Sci 119: 1122–1134, 2011

Key words: hydrogel; compression behavior; nanocomposite; mechanical properties; structure–property relationships; bentonite; swelling; friction; network

INTRODUCTION

Hydrogels are hydrophilic crosslinked polymer networks capable of swelling in water or aqueous fluids, whereby retaining a large amount of fluid in their swollen state. The water content in the equilibrium state affects the performance of the hydrogels, such as mechanical properties, surface properties, permeability, and biocompatibility. Hydrogel materials have found numerous applications (biomedical, optical, water purification, soil stabilization etc.) in the past (e.g., as shown in Ref. 1). The main feature that makes hydrogels so interesting for the integration in biological systems is their high water content. The amount of water that can be uptaken, as well as the thermal, mechanical, chemical, and optical properties are varied in function of the (co)polymerizable monomers and crosslinking agents that the hydrogels consist of (e.g., as shown in Ref. 2–4). Nowadays primary interest is devoted to stimuli-responsive hydrogels with great application potential, especially in drug delivery. However, the mechanical properties (compression, tension) of synthetic hydrogels are usually inferior to those of natural soft tissues, such as the Achilles tendon or articular cartilage. The latter can sustain large deformations in both tension and compression, despite their water content of about 90 vol %.[5] As this drawback strongly hampers the possible use of conventionally crosslinked hydrogels, considerable efforts are made to improve the hydrogels' mechanical performance.

Correspondence to: J. Karger-Kocsis (karger@pt.bme.hu).
Contract grant sponsor: European Union (Acronym: "PhotoNanoTech"); contract grant number: NMP4-ct-2007-033168.
Contract grant sponsor: German Research Foundation (DFG).

TABLE I
Chemical Composition of Hydrogel Systems Given in wt % and mol % (in Bracket), Respectively

Sample code	AMPSA	AAm	MbAAm[a]	$K_2S_2O_8$[a]	NB[a]
H	50 (74.46)	50 (25.54)	0.25 (0.17)	0.125 (0.05)	–
H-NB	50 (74.46)	50 (25.54)	0.25 (0.17)	0.125 (0.05)	4

[a] Concentration given by considering the total amount of the monomers.

The related research follows basically two ways: creation of novel type crosslinked structures (double networks, interpenetrating networks etc.) and incorporation of water swellable or dispersible nanofillers (e.g., layered silicates[6]). Key factors for application of hydrogels in the biomedical area (contact lens, catheter, artificial articular cartilage, artificial esophagus, etc.) are their low surface friction and wear rate.[7] Development of hydrogels with low coefficient of friction (COF), comparable with that of mammal joints, in the range of 0.001–0.03,[8] is a great challenge. Wear needs to be minimized and the debris produced should not be toxic.[9] However, the hydrogels usually contain about 90% water, which makes them extremely weak when subjected to mechanical, including frictional-type loads. Therefore, to gain knowledge on how hydrogel characteristics (e.g., crosslink density, water content etc.) influence the sliding friction and wear behavior is an extremely important task. Some researchers have already made attempts to study the friction and wear phenomena in hydrogels.[10,11] Gong's team systematically investigated the tribological behavior of different hydrogel systems obtained under different polymerization conditions.[12–15] They discovered that the friction coefficient of polyelectrolyte hydrogels is largely dependent on their chemical composition and charge density of the gels.[13] Furthermore, it was discovered that, even for the same chemical structure, hydrogels exhibit a much lower surface friction when they are synthesized on a hydrophobic substrate such as Teflon and polystyrene compared to the hydrogels synthesized on glassware substrates.[14] To improve the wear resistance, the reinforcement of hydrogels via incorporation of water swellable layered silicates, such as pristine bentonite, seems to be very promising. It is the right place to emphasize that the accurate testing of hydrogels is not an easy task because the inherently weak hydrogels easily break and fragment upon mechanical loading. The aim of this article was to improve the performance of hydrogels using sodium bentonite (NB) nanoreinforcement, and explore some new testing possibilities for their compression, compression creep and tribological testing. The model hydrogel belongs to the family of polyacrylamide-type versions synthesized from acrylamide (AAm) and 2-acryloylamido-2-methylpropanesulfonic acid (AMPSA) monomers.

EXPERIMENTAL

Materials

The AAm and AMPSA monomers, as well as methylene-bisacrylamide (MbAAm) served as a crosslinker, purchased from Sigma–Aldrich Chemie GmbH (Taufkirchen, Germany), were used as received. Potassium persulphate ($K_2S_2O_8$) was obtained from Merck (Darmstadt, Germany) and used as polymerization initiator. The pristine sodium bentonite (EXM 757 type, abbreviated further on by NB), which belongs to the family of natural montmorillonites, was supplied by Süd Chemie AG (Munich, Germany). Its cation exchange capacity and interlayer spacing were about 80 mequiv/100 g and 1.24 nm, respectively.

Preparation of hydrogels

One gram of AMPSA, 1 g of AAm, and 0.005 g of MbAAm were dissolved in 6 g of bidistilled water at continuous stirring. When a transparent solution was obtained, 0.0025 g of $K_2S_2O_8$ was added last. For the NB-modified hydrogels, 0.08 g of NB was firstly dispersed in water and all monomers and initiator were added to the prepared nanoparticle slurry. The concentration of solids in water was 40 wt %. The solid component ratios in reactive mixtures are presented in Table I and given as both weight and mol percentage. After the reactive mixtures were prepared, they were poured to Petri dishes and heated for 8 h at 60°C. After the synthesis, the gels were dried for 24 h at 50°C under vacuum to constant weight. The dry specimens were then submerged in distilled water for 2 weeks at room temperature to remove unreacted components, and the soluble (sol) fraction (SF, wt %) was calculated with the equation:

$$\mathrm{SF} = \frac{m_0 - m'}{m_0} \cdot 100 \quad (1)$$

where m_0 is the initial mass of dried gel after synthesis, m' is the mass of dried sample after 2 weeks immersion in water. The sol-fraction was evaluated from the triplicate measurements of each sample and was assessed as 10–12% for both hydrogels.

Swelling behavior

The swelling degree (Q, $g_{H_2O}/g_{polymer}$) was calculated by the following equation:

$$Q = \frac{m_s - m_d}{m_d} \quad (2)$$

where m_s and m_d is the weight of swollen gel and the initial weight of dry samples before swelling, respectively. The swelling behavior of the gels was investigated at 25°C in distilled water by measurement of their weight at regular time intervals. Equilibrium water content (EWC, %) in hydrogels was estimated at equilibrium swelling and was calculated as follows:

$$\mathrm{EWC} = \frac{\mathrm{m_s} - \mathrm{m_d}}{\mathrm{m_s}} \cdot 100 \quad (3)$$

The mean values of both Q, and EWC data were deduced form three parallel measurements.

Differential scanning calorimetry measurements

A Mettler Toledo DSC 821 thermal analyser was used to measure the phase transition of water absorbed by the hydrogels. The state of water was investigated for gels, swollen in equilibrium, in deionised water at 25°C, in a temperature range from −30 to 30°C at a heating rate of 2°C/min under N_2 atmosphere. The surface water was removed from the hydrogel samples with a soft paper and sealed in aluminium pans. The weight of the samples was in the range of 15–20 mg. The enthalpy of fusion of each sample was taken as a normalized value to the weight of sample. Each experiment was carried out at least twice.

Compression mechanical tests

Uniaxial compression measurements were performed on equilibrium water-swollen gels at 25°C using a Q800 dynamic mechanical analyzer (DMA of TA Instruments, New Castle) in compression mode. Hydrogel samples were cut to specimens with a diameter of 12.6 mm and thickness of 3.2 mm. All measurements have been tested for 5–6 min until break without additional wetting at a load rate of 1 N/min. To obtain statistically reliable results all measurements were performed on 10 samples of each of hydrogel system.

Compression creep tests

The compression creep behavior of hydrogel samples was tested by using two different devices providing different regimes. A Q800 dynamic mechanical analyzer (DMA of TA Instruments, New Castle, USA) in compression mode was utilized to study the creep behavior at short-term load process. Disk-shaped samples with a diameter of 12.6 mm and a thickness of 3.2 mm were cut from the equilibrium-swollen hydrogels. A compression pressure of 7 kPa was applied for 20 min; afterward, the samples were recovered for 20 min.

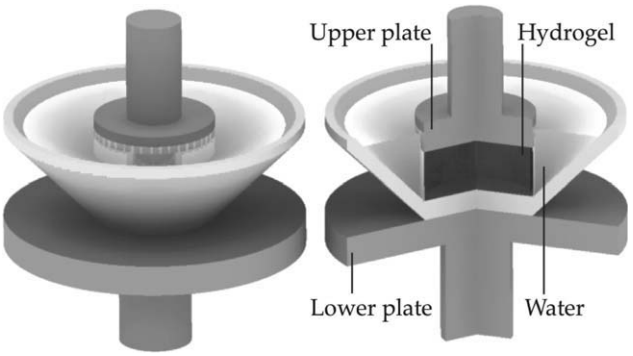

Figure 1 Schematics of the creep setup. An Al holder was placed on the lower DMA plate, and kept the sample hydrated.

A thermo mechanical analyzer (TMA 40 of Mettler Toledo, Gießen, Germany) equipped with a quartz sensor of 3 mm diameter and with a TC15 TA type controller was used for the creep tests at longer loading–deloading cycles. Disk-shaped samples with a diameter of 6 mm were cut from the equilibrium swollen hydrogels and placed in an alumina crucible with a diameter of 6.5 mm. To distribute the force on the entire surface of the hydrogels, a quartz plate with a 6 mm diameter was placed on the sample's surface and used as an expansion of the sensor. The total thickness of the aluminium holder and crucible with the plate filled with water was used as a zero point. The thickness changes of each sample were measured in the load cell and used for the calculation of sample creep deformation. The samples were subjected to three load cycles, with the relaxation load being 100 times lower than the load level: 7–0.07–7 kPa, 14–0.14–14 kPa and 18–0.18–18 kPa, the time of loading was 120 min, and the relaxation time was 240 min. A preloading phase (0.07, 0.14, and 0.18 kPa respectively) of 5 min was applied for each experiment. All creep experiments performed by both devices have been carried out at 25°C in water medium to prevent the hydrogels from drying during the experiment. For this purpose, samples were placed in a round aluminium holder filled with water, as shown in Figure 1.

Sliding friction and wear

Tribological measurements were done with a Dr. Tillwich GmbH Werner Stehr SOP 3000 tribometer in shaft-on-plate mode at room temperature (25 °C).

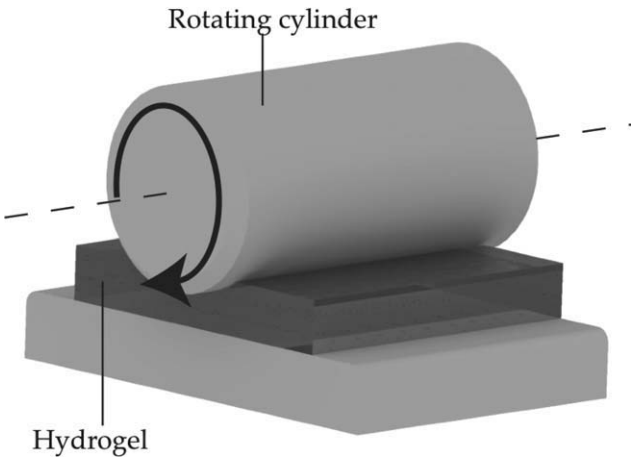

Figure 2 Schematics of the experimental setup for tribological tests. The sample was fixed on a plate and a rotating shaft pressed against its top surface. Water droplets kept the sample hydrated.

The metal shaft pressed against the hydrogel specimens with various normal loads (selected between 2.5 and 8 N), while rotating with 130 revolutions per minute (rpm) for 4 h under continuous lubrication with deionized water. The setup is shown in Figure 2. The surface roughness parameter of the steel shaft (diameter: 14.7 mm, width: 19 mm) was $R_a = 1.87$ μm.

The dynamic COF was monitored during the test continuously and was calculated by the equation:

$$\mathrm{COF} = \mathrm{F_f}/\mathrm{F_n} \tag{4}$$

where F_f is the friction force between the surfaces in contact and F_n is the normal force.

The specific wear rate was calculated by the Archard Equation:

$$W_s = W/(s \cdot P) \tag{5}$$

where W is the worn volume in mm^3, s is the sliding distance in m, P is the applied load, and W_s is the specific wear rate, i.e., worn volume per unit load per unit sliding distance. The values of W were calculated as the loss of weight of the swollen hydrogel due to the friction process. To compute W from the weight difference, the apparent densities of the swollen hydrogels were determined gravimetrically. The average values from three measurements were used to convert the wear-induced weight difference into the worn volume.

Scanning electron microscopy

The surface morphology of the specimens have been investigated by SEM using a Supra40VP Zeiss microscope with an accelerating voltage of 5 kV. Element mapping of the surfaces was performed in scanning electron microscopy-energy dispersive spectroscopy (SEM-EDS) mode with an accelerating voltage of 12 kV. Hydrogel samples were previously completely dried under vacuum and coated with an Au/Pd alloy before SEM inspection.

RESULTS AND DISCUSSION

Network parameters

One of the most important structural parameters characterizing crosslinked polymers is the average molecular mass between crosslinks, which is directly related to the crosslink density (n_c). The value of n_c significantly affects the physical and mechanical properties of crosslinked polymers, and its determination has great practical significance. Equilibrium swelling is widely used for the determination of n_c. According to the Flory-Rehner theory,[16] for a perfect network, when all chains between crosslinks are elastically effective, n_c can be determined as follows:

$$n_c = -\frac{\ln(1 - v_p) + v_p + \chi_{12} {v_p}^2}{d_p V_s ({v_p}^{1/3} - \frac{2}{f} v_p)} \tag{6}$$

where V_s is the molar volume of the solvent used for the swelling studies (water, 18.035 cm^3/mol), and χ_{12} is the Flory–Huggins interaction parameter for the polymer-solvent pair. The χ_{12} parameter value for the PAAm-PAMSA-water systems was recently evaluated[17] from the small-angle neutron scattering measurements of PAAm-PAMSA solution blends at different mol ratios. The best fit value for PAAm and PAMPSA at their mol ratio in the blend of 3 : 1 were determined as 0.45 and 0.35, respectively, so the common value for the AAm-AMPSA copolymer gel (in this work the mol ratio is also 3 : 1, see Table I) was taken assuming that the contribution of the individual component to the total χ_{12} value of a copolymer gel is proportional to their mol fractions. Next, in the equation, f is the functionality of a crosslinker (for a bis-acrylate crosslinker $f = 4$), and v_p is the volume fraction of polymer in a swollen gel, given by:

$$v_p = \left(1 + \frac{(m_{eq} - m_0) d_p}{m_0 d_s}\right)^{-1} \tag{7}$$

where d_p and d_s represent the densities of polymer and solvent, respectively, and m_0 and m_{eq} are the mass of dry hydrogels before swelling and equilibrium-swollen samples, respectively. The density of dry hydrogels has been measured gravimetrically and the average values from five measurements have been computed, as listed in Table II.

TABLE II
Physico-Chemical Characteristics of the Hydrogels

Sample code	d_p (g/cm^3)	$n_{c\ \mathrm{theor}} \times 10^6$ (mol/cm^3)	Q (g/g)	$n_{c\ Q} \times 10^6$ (mol/cm^3)	EWC (wt %)	ΔH_{endo} (J/g$_{\mathrm{gel}}$)	W_f (wt %)	W_b (wt %)	E (kPa)	$n_{c\ \mathrm{E}} \times 10^6$ (mol/cm^3)	COF (–)	W_s (mm^3/Nm)
H	0.990 ± 0.008	32.0	193.7 ± 3.2	0.49	99.49	283.6 ± 8.1	85.34	14.66	2.64 ± 0.35	5.25	0.048 ± 0.016	0.0453 ± 0.0042
H-NB	1.013 ± 0.013		109.3 ± 1.1	1.21	99.09	227.0 ± 6.8	68.59	31.12	5.39 ± 1.09	10.47	0.036 ± 0.008	0.0033 ± 0.0005

The theoretical crosslink density, $n_{c\ \mathrm{theor}}$, was obtained based on the following equation[17]:

$$n_{c\ \mathrm{theor}} = \frac{Cf}{2} \tag{8}$$

where C is the molar concentration of the crosslinking agent with functionality f. For these systems, the tetrafunctional crosslinker (MbAAm) was used, so $f = 4$.

Experimental investigations of the swelling behavior of AMPSA-containing gels at various mol concentrations[18] showed that, when the amount of AMPSA units in copolymeric gel composition is in the range of 20–60 mol %, the fraction of counterions affecting the swelling is negligibly low. In such cases, according to the Flory-Rehner theory,[16] all the counterions inside the gel are not effective in the gel swelling, and the swelling degree can be determined as that for the nonionic gels. Based on these experimental results,[18] and having a mol fraction of AMPSA in copolymer composition of gels as 25.54 mol % (Table I), it was suggested not to take into account the influence of ionizable groups of AMPSA when calculating the swelling degree of the copolymer hydrogels.

The results obtained demonstrate that NB-modified hydrogels exhibit a lower swelling degree, thus higher crosslink density than the unmodified ones. This indicates the formation of additional crosslink-joints, which is possible due to the attachment of macromolecular chains on the exfoliated platelets of inorganic clay. Such effects have also been described by other researchers.[19,20] In the cited works, nanocomposite poly(*N*-isopropyl acrylamide) (PNIPA) hydrogels were formed using inorganic clay as a multifunctional crosslinker through noncovalent interactions with polymer chains.[19] Furthermore, such attachment was also traced to radical reactions occurring at the clay surfaces due to the association of the initiator ($K_2S_2O_8$) with clay by ionic interactions in the corresponding solution.[20] As a result, the polymer chains attached to the clay platelets form additional crosslinking centres. In this work, taking into account the presence of ionic AMPSA in hydrogels, it may be assumed that both effects, i.e., ionic interactions and radical reactions, can take place. It is noteworthy that NB was mostly exfoliated in the corresponding hydrogel. This can be deduced from the fact that not even the dried H-NB sample showed any obvious peak in the corresponding X-ray diffraction spectrum at low scattering angles (not reported here).

On the other hand, both of the hydrogels demonstrate much lower crosslink density than expected from the theoretical approach, considering the mol concentration of crosslinker per volume unit of network ($n_{c\ \mathrm{theor}}$, Table II). This suggests the formation of an imperfect network in the hydrogels. This is in

line with the rather high amount of the soluble fraction (SF = 10–12 %). In addition, it should be borne in mind that the efficiency of MbAAm is between 50 and 64%.[21]

Swelling kinetics

Swelling kinetics is a very important characteristic of hydrogels, as it provides information on the diffusion character and velocity of water sorption, as well as the time needed until equilibrium state is reached.

Typical swelling curves (Q vs. time) of the clay-free hydrogel and its bentonite reinforced version are presented in Figure 3(a). It can be seen that the unmodified hydrogel reaches equilibrium during the first 80 h and demonstrates a high swelling degree (up to 200 g of water per 1 g of dry polymer, Table II). However, after modification the swelling ratio of NB-modified hydrogel is almost two times lower and at the same time its swelling rate is significantly higher. The lower water uptake of H-NB gel is evidently due to the enhanced crosslink density. Similar behavior was also observed by Kabiri's research group, when introducing chitosan-modified montmorillonite (MMT) into the poly(AMPSA)-based gels up to 6%,[22] or kaolin into poly(acrylic acid)-based hydrogels.[23]

To investigate the mechanism of diffusion of water molecules within the gels, the initial swelling data were fit to the equation:

$$Q(t) = kt^n \tag{9}$$

where $Q(t)$ is the measured swelling ratio at time t, k is the swelling rate front factor, and n is the kinetic exponent. This equation is a phenomenological law, in which n is related to the type of sorption mechanisms of hydrogels. When n is equal to 0.5, it indicates Fickian diffusion (Case I), which is characterized by a solvent diffusion rate much slower than that of the polymer relaxation. The other extreme, when $n = 1$, indicates non-Fickian (Case II) diffusion, where the diffusion process is faster than the relaxation rate. Another case of non-Fickian diffusion (anomalous) describes the cases where the diffusion and relaxation rates are comparable, so $n = 0.5$–1.[24] The value of n can be obtained as a slope from the double logarithmic plot of swelling ratio (Q) vs. time of swelling (t), in the linear part of swelling curve, and in our case this time interval is 10 h.

As it is shown in Figure 3(b), the value of n was determined as 0.74 for the initial H-gel and 0.64 for the modified H-NB gel suggesting the non-Fickian anomalous mechanism of water sorption for both gels. Such swelling behavior is typical for ionic gels[25] and is caused by their large affinity toward water due to the repulsive forces between the ionizable groups. However, it is seen that NB-modified hydrogel swells faster than the reference [Fig. 3(a)], and its diffusion is closer to Case I than that of the pristine gel [Fig. 3(b)]. This fact may be explained by the presence of strongly hydrophilic clay which attracts water at the beginning of swelling much faster. This is accompanied by a faster relaxation of polymer chains between crosslinks due to their shorter length (crosslinking degree of H-NB is higher; therefore, the mean molecular weight of macromolecules between the crosslinks is lower).

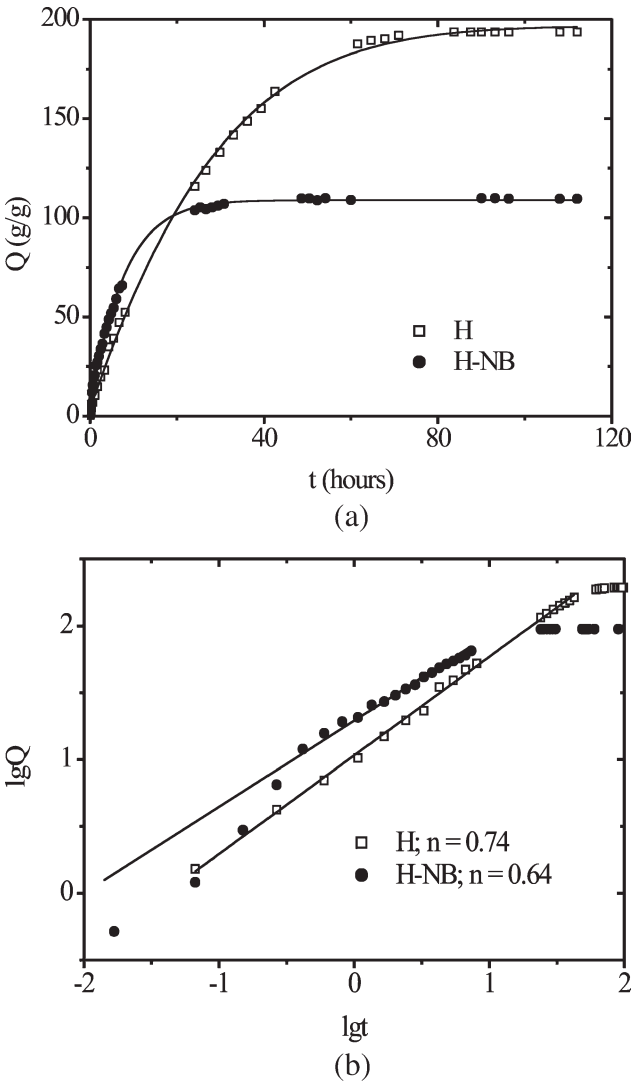

Figure 3 Water uptake curves (a) and their double logarithmic representations (b). Notes: slopes are fitted to the linear region of the swelling curve. The kinetic exponent, n, is depicted in the legend.

Water state characterization

The Differential scanning calorimetry (DSC) method is extensively used to get information on the interaction of water and polymers in the hydrated state of the latter.[26–28] Investigators differentiate between at

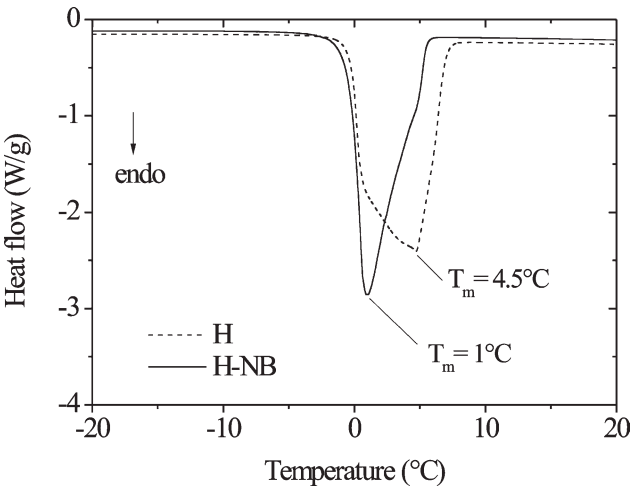

Figure 4 DSC curves of swollen hydrogels.

least three types of water in swollen polymers: free water (water with the same freezing point as bulk water, i.e., near to 0°C), freezing bound water (water freezing at a temperature much lower than 0°C), and nonfreezing bound water (water that does not form ice at all and therefore cannot be detected directly by calorimetry).[26] DSC analysis allows to estimate the amount of freezable (free and freezing bound) water from enthalpies of its phase transitions (melting/crystallization) quantitatively. In this work, the DSC analysis of water-swollen gels was carried out during the heating process.

As no endothermic peaks were observed in the region below 0°C (Fig. 4), and considering the fact that the detection of different types of freezable water (and their melting enthalpy) is significantly affected by the annealing period before DSC scanning,[27] it was suggested that there is no freezable bound water in our gels. So, the phase transition was assigned to the melting of free water. Its amount in the gels was evaluated from the melting enthalpies using the following equation:

$$W_f = \frac{\Delta H_{\text{endo}}}{\Delta H_{\text{ice}}} \cdot 100 \tag{10}$$

where ΔH_{ice} is the enthalpy of fusion of pure water (334 J/g), ΔH_{endo} is the enthalpy values associated with melting peaks of freezable water in gels determined as an area under the melting peak from DSC data.[28] The amount of bound water was evaluated from the assumption that equilibrium total water content represents the sum of the amount of freezable and nonfreezable water:

$$W_b = \text{EWC} - W_f \tag{11}$$

where W_b is the amount of nonfreezing bound water. The results of EWC, enthalpy value, and calculated amount of free and bound water related to the weight of the dry polymer in the hydrogels are presented in Table II.

From the data obtained, it can be seen that both H and H-NB hydrogels contain very high amounts of water (more then 99%), which correlates with their high hydrophilicity. However, in spite of the insignificantly lower water content of H-NB gel (99.09 % compared to 99.49% of H-gel, see Table II), its enthalpy of melting is notably lower than that of the reference gel (227 J/g compared to 283.6 J/g for the pristine gel). This indicates a considerably lower content of freezable water in the H-NB system (Table II). Because of the presence of ionic functional groups of AMPSA, the amount of bound water was rather high and was found to be 14.66% for the clay-free gel. Modification by 4 wt % NB significantly increased the content of bound non-freezable water, i.e., up to 31.41%. It should also be noted that the temperature of ice melting determined from DSC curve of the NB-modified gel is notably lower than that for the H-gel (4.5 compared to 1°C, see Fig. 4). Such a depression in the melting point demonstrates a more bonded state of freezable water in a clay-modified hydrogel matrix compared to the parent gel. Accordingly, the water state was influenced markedly by the inorganic clay. These results indicate a strong interaction of water molecules with the clay layers, and these interactions were not destroyed during the hydrogel formation. This fact may significantly influence the mechanical and tribological properties of clay-modified hydrogels.

Mechanical properties of the hydrogels

The stress–strain curves of uniaxial compression tests of equilibrium swollen at 25°C hydrogels are presented in Figure 5(a), whereas Figure 5(b) shows the initial part of experimental curves at small deformations. As seen in Figure 5(a), the incorporation of 4 wt % NB increased the ultimate compression strength (σ) at break from 20 to 35 kPa; however, at the same time, it slightly reduced the corresponding strain (from 60 to 50%) compared to the unmodified gel. This indicates a significant improvement in the compressive mechanical properties due to the clay modification. The slight reduction of strain is obviously due to the higher network density of NB-modified gel, and to the lower amount of water, that makes the gel stronger. An additional straightforward explanation is that the exfoliated/intercalated bentonite layers may change their orientation under loading, while enhancing the maximum (or critical where the hydrogel breaks apart) stress.

In the swollen state, most hydrogels demonstrate a rubber-like elastic behavior with a rapid rearrangement of the polymer segments under external

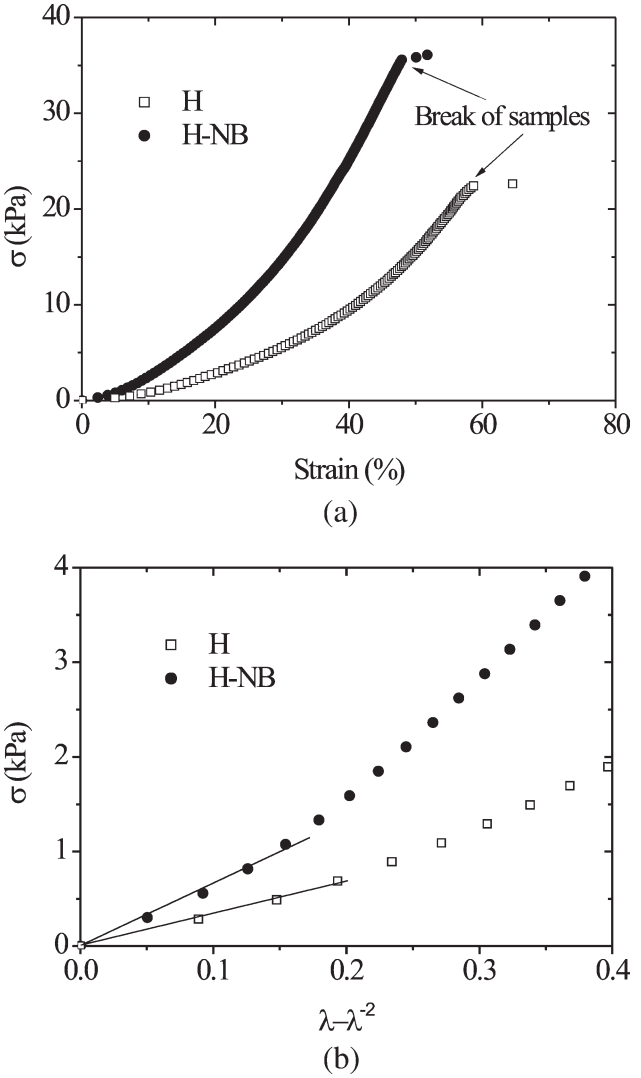

Figure 5 Typical DMA compression stress–strain curves (a) and the straight lines fits to the experimental data in the initial deformation range (represents the elastic modulus E) (b). Note: data presented are linked with the average from 10 experiments for each gel.

stresses. In such a state, the mechanical behavior of gels is dependent mainly on the architecture of the polymer network. Then, the elastic modulus, E, can be determined from the slope of the linear dependence in the following equation:

$$\sigma = E(\lambda - \lambda^{-2}) \tag{12}$$

where σ is the applied compressive stress, λ is the relative deformation:

$$\lambda = L/L_0 \tag{13}$$

where L is the deformed thickness and L_0 is the initial thickness of a sample before deformation.[29] The fitted lines used for the determination of E as their slope value are shown in Figure 5(b). The elastic modulus correlates with crosslink-density of swollen network (n_c) as follows:

$$E = RTv_p n_c \tag{14}$$

where R is the universal gas constant, T is the temperature, v_p is the volume fraction of polymer in swollen gel, and n_c is the concentration of crosslink joints per unit volume. It should be noted that this approach of crosslink density determination does not consider the molecular structure of the gel and its interaction with the solvent and is concerned only with the observed macroscopic behavior of the system.

Comparing the results obtained for the hydrogels' crosslink density by two approaches (using equilibrium swelling ($n_{c\ Q}$) and elastic modulus ($n_{c\ E}$) for calculations, Table II), it can be seen that the crosslink density determined via elastic modulus is about 10 times higher than that determined by swelling. This can be explained by the fact that these two methods reflect different properties of the hydrogels. As mentioned above, the mechanical approach does not take into account the chemical nature of hydrogel network, its affinity to solvent (water here), or electrostatic forces in ionic hydrogels. However, for the clay-modified gels during swelling, the interaction of bentonite with water was not taken into account. This interaction may change the Flory-Huggins parameter χ_{12} and influence the calculated n_c. On the other hand, the modulus of elasticity is mainly influenced by the number of elastically effective chains of the hydrogel network and, very significantly, by the entanglements and micro-heterogeneities of the network, which are typical for this kind of hydrogels.[30] So, from a practical viewpoint, the determination of the network density from mechanical tests is favorable. It should be noted that the values of n_c, determined from the mechanical tests, are also much lower compared to the theoretical crosslink density. Similar effects were observed by other scientists, as well.[21]

Sliding friction and wear

Figure 6 shows the time profiles of the COF of the hydrogels investigated. As it can be seen for H-gel, its COF is very low in spite of the relatively high roughness of the metallic shaft counterpart (Table II). Very low values of COF for AAm-AMPSA-based hydrogels have already been reported by Gong et al.[12,13] and were attributed to the strong repulsive forces of negatively charged ionic groups of AMPSA. They also reported that friction coefficient tends to decrease when raising the charge density of a surface of ionic hydrogels.[13]

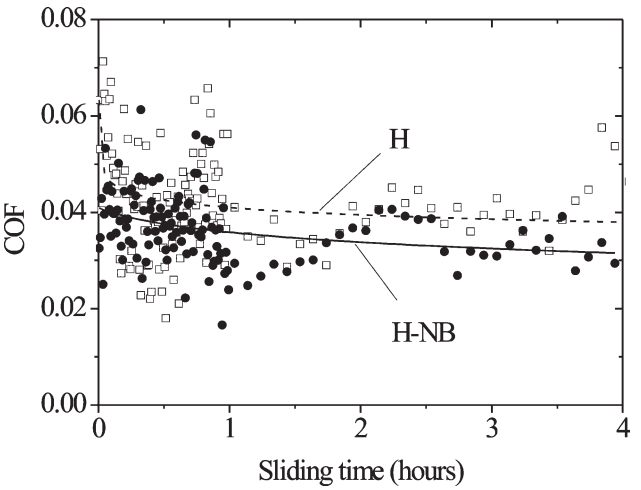

Figure 6 Tribological behavior of the reference (H, open symbol) and bentonite-modified hydrgels (H-NB, filled symbol). Solid curves represent the fits with experimental data.

The friction of the 4 wt % NB gel was unexpectedly low, in spite of the significantly lower swelling ratio (Table II). A decrease of COF for clay-modified hydrogels was also observed by Haraguchi and Takada.[31] This was assigned to dangling of uncrosslinked polymer chain ends from exfoliated clay platelets, which affected the interface and reduced the friction under wet conditions. On the other hand, this behavior may be related to changes in the surface properties of the hydrogels. The presence of clay nanoparticles at the gels' surface can rearrange and alter the surface polarity and morphology. This is accompanied by a change in the surface tension, which can reduce the friction. However, this hypothesis requires further experiments.

The specific wear rate (W_S) is remarkably lower for the NB-modified hydrogel when compared with that of the reference (Table II). This suggests a reinforcing effect of NB due to the strong adsorption of polymer chains on the filler surface, and strong H-bond interactions between the hydroxyl groups of the bentonite (at its surface) and functional groups of the copolymer network (carbonyl and amino groups of AAm and AMPSA, respectively). All this increases the apparent crosslink degree. Thus, improvement in the compression mechanical properties of NB-modified hydrogel due to the nanofiller reinforcement is associated, at the same time, with a higher resistance to sliding wear.

Creep behavior

In general, hydrogels are not simply elastic materials but behave viscoelastically and mechanical deformation leads to a time dependence on the applied stress due to the movement of polymer chains segments. This movement induces an internal response, resulting in a time-dependent recovery when the external load is removed. Thus, the time dependence of the applied stress or strain is as important as the prediction of the material's mechanical response. The investigation of the creep behavior makes the determination of the viscoelastic and viscoplastic responses possible. In this work, the initial and NB-reinforced hydrogels were subjected to creep tests. The total deformation of hydrogels (ε) after the load-cycle was calculated as a ratio of thickness at the end of loading to the initial thickness of the samples. Additionally, the plastic (irreversible) deformation (δ) was estimated as the strain value at the end of the recovery-cycle. The DMA method was applied at a relatively short load-cycle setting and TMA tests were carried out under several load-conditions with increased durations for both load and relaxation cycles.

Representative DMA creep and relaxation curves are presented in Figure 7. At the beginning, the samples responded elastically to the initial mechanical load yielding at 30 and 23% strain values for the H and H-NB gels, respectively. After 20 min of loading, the related strain (ε) values reached 33 and 27% for H and H-NB, respectively (Table III). When the load was removed, the strain dropped suddenly to 2.5–3% and within 3–4 min the initial thickness of the specimens was practically restored and δ was found to be 0% for both H and H-NB gels. Such fast response of hydrogels to load changing conditions was also observed by other investigators.[32]

Results of creep tests carried out by TMA at different load conditions are presented in Figure 8. The value of elastic (reversible) deformation (έ) was evaluated as the difference between ε and δ at the first

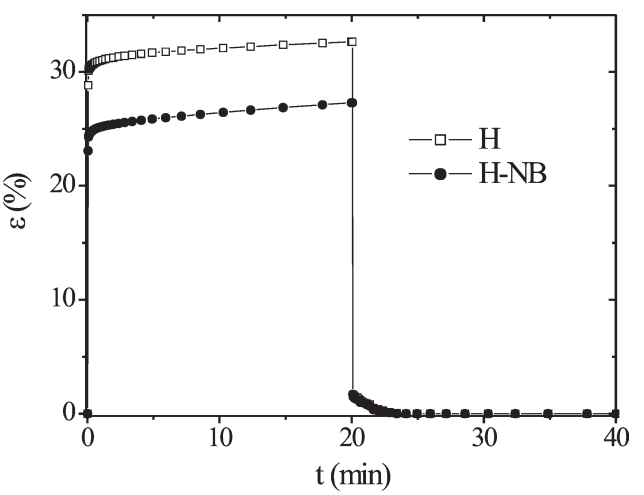

Figure 7 Compression creep and relaxation for the hydrogel samples in DMA. Notes: the applied load was 7 kPa before deloading. The duration of both loading and deloading was 20 min.

TABLE III
Creep Characteristics of the Hydrogels

Sample code	Load (kPa)	DMA (load/relaxation: 20/20 min)			TMA (load/relaxation/load: 120/240/120 min)		
		ε (%)	δ (%)	ε (%) 1st cycle	δ (%)	έ (%)	ε (%) 2nd cycle
H	7	32.6 ± 0.9	0	43.0 ± 1.1	2.0 ± 0.2	41.0 ± 1.3	43.5 ± 1.0
	14	–	–	51.5 ± 1.3	2.5 ± 0.2	49.0 ± 0.9	53.9 ± 1.2
	18	–	–	72.0 ± 1.0	65.0 ± 0.7	7.0 ± 0.4	[a]
H-NB	7	27.3 ± 1.0	0	38.5 ± 0.6	1.5 ± 0.1	37.0 ± 0.6	39.9 ± 0.4
	14	–	–	41.0 ± 1.3	3.0 ± 0.12	38.0 ± 1.2	42.1 ± 1.5
	18	–	–	57.8 ± 1.2	5.0 ± 0.5	52.8 ± 1.7	58.0 ± 1.2

[a] Sample already destroyed.

load-cycle. Results obtained at low load (7 kPa) are in good agreement with DMA creep data. However, longer load times (120 min instead of 20 min) resulted in higher deformation (Table III). Similarly to the DMA creep behavior, after deloading, both hydrogels recovered relatively fast: in 5 min the residual deformation was 4–5% and then, in 240 min of relaxation, it was further reduced to 1.5–2%. As it can be seen, the plastic deformation after the first 120 min load-cycle is higher than that determined by DMA in a shorter loading time for both hydrogel systems. These results indicate that longer loading time leads to more irreversible deformation in the hydrogels. As expected, when increasing the compression loads, the creep deformation rises for both gels, and the creep is maximal under 18 kPa. At the same time, for the H-NB gel, the deformation is lower compared to the unmodified H-gel under all loading conditions. This is in good agreement with DMA creep investigations (Table III). It is also seen that plastic deformation increases with the loading force. At 18 kPa load, the plastic deformation is very high (65%) for the reference H-gel, indicating its weak compression resistance (the gel network is already significantly destroyed). However, the modification of the hydrogel with 4 wt % NB significantly improved the creep behavior. For example, the irreversible deformation was found to be 5% in the 18 kPa creep load regime. After the second load-cycle, the final deformation of the hydrogels is higher than after the first loading. This confirms some destruction of the gel network due to the first loading cycle. However, for the clay-reinforced samples, the deformation after the second load-cycle changed insignificantly. These results indicate significant improvement of their compression resistance against "long-term" deformations due to the reinforcement of AAm-AMPSA hydrogels by inorganic clay. Recall that this modification had no negative impact on the COF (as discussed in section above) in spite of the lower water content.

SEM investigations

The surface morphology of the hydrogels after drying is presented in Figure 9. The slight surface waviness of the reference system detected at higher magnifications may be explained by a nonuniform contraction of the hydrogel during drying. Significant changes in the surface morphology of the samples were observed after the NB modification of the hydrogel. The dispersion of uniformly sized clay particles is well resolved (SEM pictures in the bottom line of Fig. 9). Although the NB filler was well dispersed in the matrix, the presence of larger agglomerates with sizes up to 10 μm could also be detected. This agglomeration probably represents the nonexfoliated (i.e., intercalated) portion of the

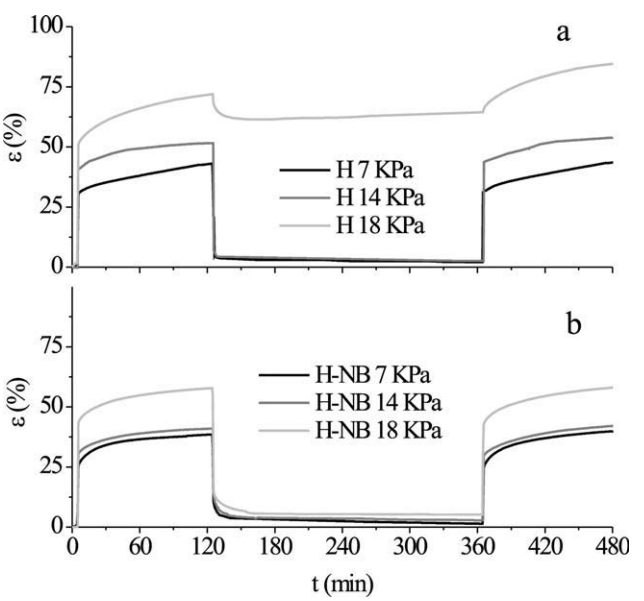

Figure 8 Compression creep and relaxation behavior of H-reference (a) and H-NB (b) hydrogels under different loading conditions in a TMA device. Note: the applied load is depicted in the legend.

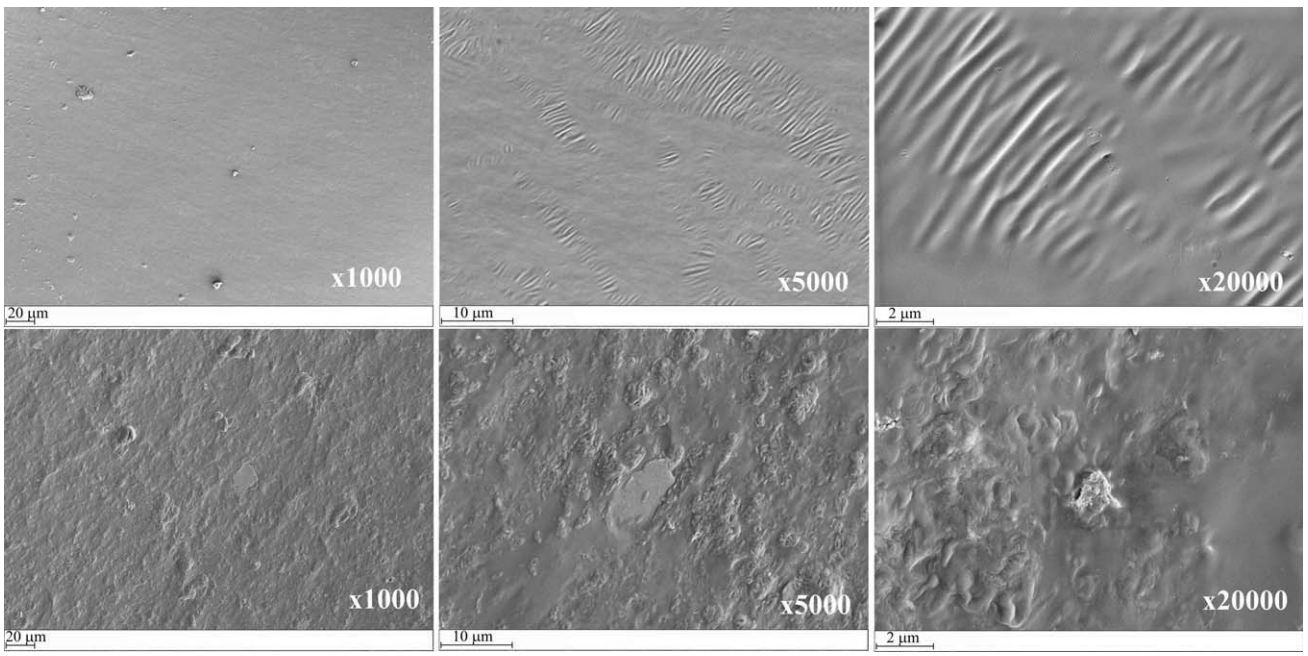

Figure 9 SEM images of the dried surfaces of H-reference (top) and H-NB (bottom) hydrogels at different magnifications.

NB. Note that the formation of agglomerates may also be triggered during the drying of the hydrogel.

Figure 10(a) demonstrates that the reference H-gel is transparent in equilibrium swollen state. However, the NB modification makes the hydrogel slightly hazy [Fig. 10(b)] compared to the reference. This suggests the presence of microscaled agglomerates in the H-NB system. On the other hand, SEM pictures demonstrate the good bonding between the filler and polymer matrix (cf. Fig. 9). The latter is due to the strong interaction of the polymer functional groups with the absorption centers (OH-groups) of the clay platelets via H-bonding. Chemical reactions between the $-SO_3H$ group of AMPSA and the metallic structural components of the clay cannot be excluded, either. Moreover, ionic interactions between the SO_3^- anions of AMPSA and clay cations (i.e., Na^+) may also be present. These interactions cause the reorganization of polymer chains near the filler particles and change the surface morphology of the clay-reinforced hydrogel. This fact may be a reason for the significant improvement of the mechanical properties and resistance to sliding wear compared to that of the pristine gel.

To investigate the structural changes of the hydrogels' surface due to the filler in more detail, the

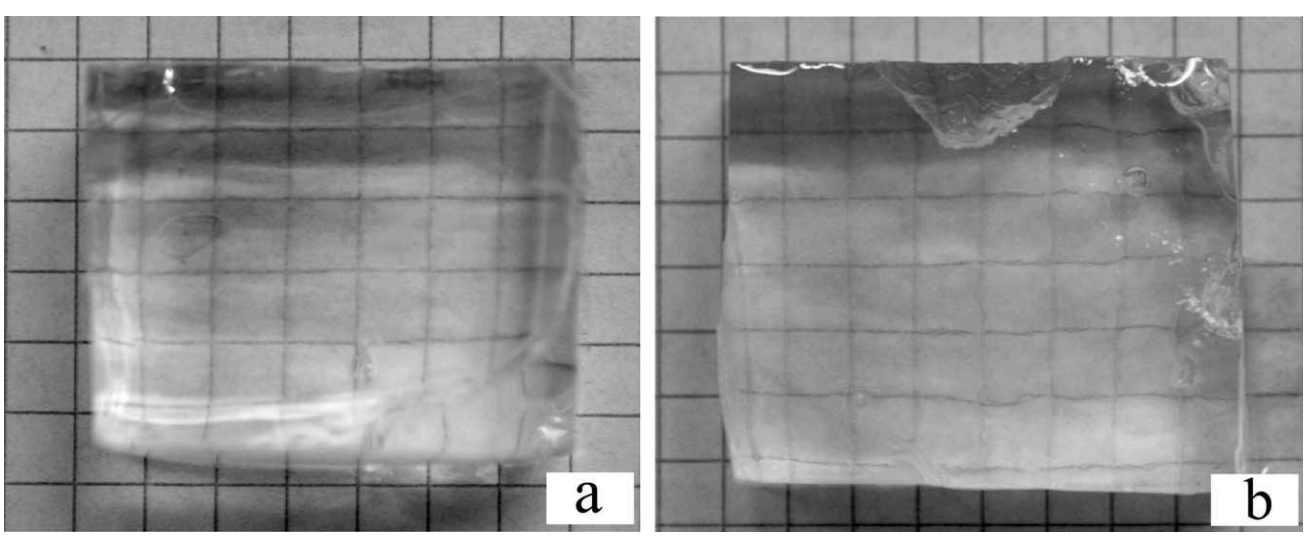

Figure 10 Photos of the swollen H (a) and H-NB (b) hydrogels.

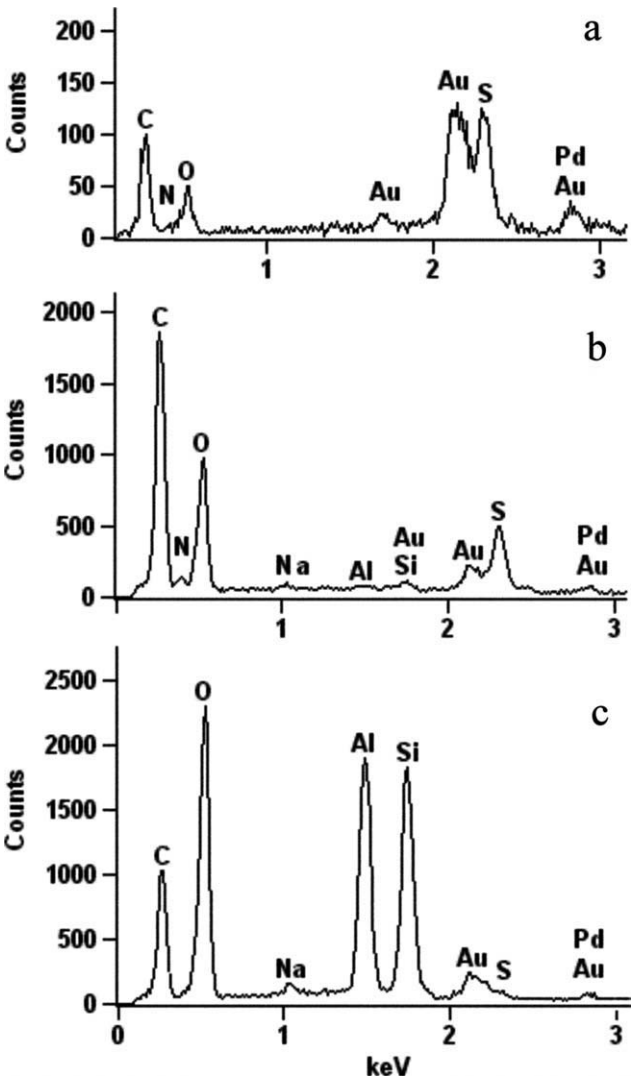

Figure 11 SEM-EDS spectra acquired from the surfaces of dried H (a) and H-NB (b and c) hydrogels. Notes: spectra b and c were taken from surfaces of H-NB with uniform clay dispersion and from a clay-rich agglomerate, respectively. Au and Pd peaks are owing to the conductive surface coating.

dried hydrogel samples were subjected to SEM-EDS analysis, i.e., for element mapping of their surfaces. The results obtained are presented in Figure 11. Although all specimens were covered by conductive Au/Pd alloy, the intensity of the characteristic peaks of the H-reference sample was very low [Fig. 11(a)] due to the low conductivity of organic matrix. However, it can be clearly seen that sulfur and carbon are the dominant elements in the spectrum, which indicates that sulfonated units of AMPSA are mostly localized on the sample's surface. For the bentonite-modified sample, the element analysis of the surface areas free of clay agglomerates [Fig. 11(b)] demonstrates a redistribution of elements compared to the H-sample. The presence of the peaks that are typical for NB (Na, Al, and Si) confirms the existence of nanosized clay platelets, uniformly distributed in the H-NB matrix, and their low intensity is probably due to the low concentration of NB on the surface. It is interesting to notice that the peak intensity ratios of carbon/sulfur, oxygen/sulfur and nitrogen/sulfur elements increased from about 1, 0.5, and 0.1 for H-reference to about 20, 2, and 0.2, respectively, for the H-NB hydrogel. This suggests that instead of AMPSA-units now AAm-units are mostly present at the specimens' surface. The AMPSA-units are mainly in close vicinity of the clay particles due to strong ionic interactions. The latter can be confirmed by the detection of sulfur and carbon peaks on the surface of clay agglomerates [Fig. 11(c)]. The higher intensity of the oxygen peak here is obviously derived from the NB structure and is due to the additive effect of organic (in structure of the sulfonated units) and inorganic (in structure of the clay) oxygen atoms. It should be noted that the higher intensity of the recorded peaks for the NB-modified sample [Fig. 11(b,c)] should be attributed to the higher conductivity of the sample's surface. This fact clearly indicates an increase in the surface charge density, which may play an important role in the reduction of the COF. Moreover, the localization of $-SO_3H$ containing units on the NB surface can be another reason for the decrease of the COF, in addition to the reinforcing effect of NB (decreasing the wear rate) when comparing to the H-reference. This assumption is based on literature data reporting that the incorporation of sulfonated monomers in acrylic based hydrogels decreased their COF.[12,13]

CONCLUSIONS

Based on this work devoted to study of the effects of sodium bentonite (NB added in 4 wt %) modification on the swelling, mechanical and sliding wear properties of a hydrogel synthesized from acrylamide (AAm) and 2-acryloylamido-2-methylpropanesulfonic acid (AMPSA) monomers (weight ratio: 1/1) and methylene-bisacrylamide crosslinking agent, the following conclusions can be drawn:

a. Network structure and morphology: The crosslink density, derived from swelling and compression tests, was below that of theoretical value. The incorporation of NB increased the apparent crosslink density of the related hydrogel. This was traced to the formation of additional crosslinks via covalent and ionic interactions between the clay and matrix forming monomers. NB also affected the surface composition of the related hydrogel according to the SEM-EDS results.

b. Water uptake and content: The NB incorporation caused a slight reduction of the water content but a markedly high decrease in the water uptake. This was attributed to an enhancement in the

apparent crosslink density. The swelling was faster in the presence of NB, which was explained by a difference in the hydration behaviors of the clay modified and the pristine hydrogel copolymers. The swelling kinetics of the hydrogels with and without NB showed characteristics between Fickian and non-Fickian behaviors affected by the NB presence. According to the DSC results, the incorporation of NB yielded a pronounced increase in the nonfreezing bound water content.

c. Compression mechanical properties: The addition of NB strongly improved the compression strength which was accompanied by a slight reduction in the ultimate strain. This was attributed to a higher apparent crosslink density of the modified hydrogel, and its nanoscaled reinforcement by clay platelets. The latter effect turned out to be most evident in the compression creep experiments. The elastic recovery was faster, the irreversible deformation substantially lower, and the creep loadability prominently higher for the clay-modified hydrogel when compared with the parent one.

d. Sliding friction and wear: The incorporation of NB reduced both the COF and the specific wear rate in water lubricated tests. This was traced by compositional changes in the surface layer of the hydrogel, and the reinforcing action (enhancement in the apparent crosslink density and nanoplatelet-type reinforcement) of NB.

References

1. Kopecek, J.; Yang, J. Y. J Polym Int 2007, 56, 1078.
2. Hoffman, A. S. Adv Drug Delivery Rev 2002, 54, 3.
3. Drury, J. L.; Mooney, D. J. Biomaterials 2003, 24, 4337.
4. Peppas, N. A.; Hilt, J. Z.; Khademhosseini, A.; Langer, R. Adv Mater 2006, 18, 1345.
5. Gabler, S.; Stampfl, J.; Koch, T.; Seidler, S.; Schuller, G.; Redl, H.; Juras, V.; Tratting, S.; Weidisch, R. Int J Mater Eng Innov 2009, 1, 3.
6. Vicosa, A. L.; Gomes, A. C. O.; Soares, B. G.; Paranhos, C. M. Express Polym Lett 2009, 3, 518.
7. Crockett, R. Tribol Lett 2009, 35, 77.
8. Gong, J. P.; Kagata, G.; Iwasaki, Y.; Osada, Y. Chin J Polym Sci 2000, 18, 271.
9. Davim, J. P.; Marques, N. Tribol Lett 2001, 11, 91.
10. Matzelle, T. R.; Herkt-Bruns, C.; Heinrich, L. A.; Kruse, N. Surf Sci 2000, 454, 1010.
11. Ishikawa, Y.; Hiratsuka, K.; Sasada, T. Wear 2006, 261, 500.
12. Gong, J.; Higa, M.; Iwasaki, Y.; Katsuyama, Y.; Osada, Y. J Phys Chem B 1997, 101, 5487.
13. Gong, J.; Iwasaki, Y.; Osada, Y.; Kurihara, K.; Hamai, Y. J Phys Chem B 1999, 103, 6001.
14. Kagata, G.; Gong, J. P.; Osada, Y. J Phys Chem B 2003, 107, 10221.
15. Kaneko, D.; Tada, T.; Kurokawa, T.; Gong, J. P.; Osada, Y. Adv Mater 2005, 17, 535.
16. Flory, P. J. The Principles of Polymer Chemistry; Cornell University Press: Ithaca, New York, 1953.
17. Tominaga, T.; Tirumala, V. R.; Lee, S.; Lin, E. K.; Gong, J. P.; Wu., W. J Phys Chem B 2008, 112, 3903.
18. Durmaz, S.; Okay, O. Polymer 2000, 41, 3693.
19. Haraguchi, K.; Farnworth, R.; Ohbayashi, A.; Takehisa, T. Macromolecules 2003, 36, 5732.
20. Ma, J.; Zhang, L.; Fan, B.; Xu, Y.; Liang, B. J Polym Sci B 2008, 46, 1546.
21. Aouada, F. A.; Guilherme, M. R.; Canpese, G. M.; Girotto, E. M.; Rubira, A. F.; Muniz, E. C. Polym test 2006, 25, 158.
22. Kabiri, K.; Mirzadeh, H.; Zohuriaan-Mehr, M. J.; Daliri, M. Polym Int 2009, 25, 1252.
23. Kabiri, K.; Zohuriaan-Mehr, M. J. Polym Adv Tech 2003, 14, 438.
24. Firestone, B. A.; Siegel, R. A. J Appl Polym Sci 1991, 43, 901.
25. Lee, W.-F.; Chiu, R.-J. J Polym Res 2002, 9, 141.
26. Yoshida, H.; Hatakeyama, T.; Hatakeyama, H. J Therm Anal 1992, 40, 483.
27. Roorda, W. J Biomater Sci Polym Edn 1994, 5, 383.
28. Pissis, P.; Kyritsis, A.; Ferrer, G. G.; Pradas, M. M.; Ribelles, L. G. Subsurf Sensing Technol Appl 2000, 1, 417.
29. Anseth, K. S.; Bowman, C. N.; Brannon-Peppas, L. Biomaterials 1996, 17, 1647.
30. Okay, O.; Durmaz, S. Polymer 2002, 43, 1215.
31. Haraguchi, K.; Takada, T. Macromol Chem Phys 2005, 206, 1530.
32. Lopatin, V. V.; Askadskii, A. A.; Preegudov, A. S.; Vasil'ev, V. G. J Appl Polym Sci 2005, 96, 1043.